Applied Catalysis B: Environmental 95 (2010) 439–445

Contents lists available at ScienceDirect

Applied Catalysis B: Environmental

journal homepage: www.elsevier.com/locate/apcatb

# Photocatalytic isomerization of norbornadiene to quadricyclane over metal (V, Fe and Cr)-incorporated Ti–MCM-41

Ji-Jun Zou *, Yi Liu, Lun Pan, Li Wang, Xiangwen Zhang

*Key Laboratory for Green Chemical Technology of Ministry of Education, School of Chemical Engineering and Technology, Tianjin University, 92 Weijin Road, Nankai District, Tianjin 300072, China*

ARTICLE INFO

*Article history:*
Available online 25 January 2010

*Keywords:*
Norbornadiene
Quadricyclane
Photocatalyst
M–Ti–MCM-41
Photoisomerization

ABSTRACT

The photoisomerization of norbornadiene using M–Ti–MCM-41 (M = V, Fe and Cr) has been studied to develop an alternative for solar energy accumulation and high energy aerospace fuel synthesis. The photocatalysts were prepared via hydrothermal method and characterized by EDX, XRD, $N_2$ adsorption–desorption, TEM, UV–vis, XPS and IR. With the same Si/M ratio in starting materials, the final concentration of V in the photocatalyst is significantly lower than that of Fe and Cr. $V^{5+}$ and $Fe^{3+}$ ions are highly dispersed in Si–O framework with tetrahedral coordination when the metal content is low, and the ordered structure is well retained. However, some species in higher coordination and polymerized environments present with increasing metal content, and the ordered structure becomes to collapse. Cr ions are difficult to get into the framework with various species like extraframework $Cr^{6+}$ and bulk $Cr_2O_3$ formed, also the ordered structure is greatly destroyed. Under UV irradiation, the transition metal ions can improve the photoisomerization activity, with the order of V > Fe > Cr. The activities of V– and Fe–Ti–MCM-41 rise with the increase of Si/M ratio, whereas the performance of Cr–Ti–MCM-41 is irregular. The photocatalysts do not exhibit any activity under visible light, regardless of their absorption in visible-light region. The activity is closely related to the extent of dispersion and local structure of metal ions, about which an indirect excitation process of Ti–O species is suggested.



## 1. Introduction

Solar energy accumulation and transformation has attracted great interest because the problem of depleting natural energy sources is becoming ever more critical. One of the approaches utilizing solar energy is to accumulate it as strain energy in metastable photoinduced isomers of organic compounds. The photoisomerization of norbornadiene (NBD) is very promising for this purpose [1–7]. When 1 mol of NBD is transformed into quadricyclane (QC), 89 kJ energy can be stored. Under some catalytic conditions, the inverse QC → NBD transformation occurs easily, accompanied with considerable thermal effect. Although there is a wide range catalysts enabling the heat release, the activation barrier for thermal QC → NBD transformation is very high [1,8,9], which makes it possible to store the accumulated energy for a long time.

QC is endowed with high energy content by the extraordinarily high strain energy [10]. Moreover, it is thermally stable enough to be stored and transported in the same way like refined hydrocarbons. These advantages make it a potential high-energy replacement or additive of current hydrocarbon-based propellants. Actually, there are many literatures aiming to utilize QC-based propellants for aerospace propulsions [11–14].

The photoisomerization of NBD is generally conducted with the presence of sensitizers, as to which many aspects including sensitizer synthesis, reaction optimization and quantum mechanism have been studied [1–9]. However, the photosensitized reaction suffers from some drawbacks. First, the sensitizers are soluble in the reaction mixture, thus a difficulty arises in product purifying and sensitizer recycling. Second, the sensitizers are prone to decomposition under irradiation that causes some undesired side reactions. With these considerations, we have suggested an alternative route using semiconductors. $TiO_2$ was found to be able to facilitate the photoisomerization of NBD but the activity is relatively low, and doping metal ions like Zn and La could enhance the activity [15]. We also incorporated Ti into MCM-41, discovering that isolated Ti–O moieties in Si–O framework were more active than the polymerized and bulk species [16].

Transition-metal-incorporated MCM-41 generally shows high photocatalytic activity due to the high dispersion of photoactive sites and effective separation of electrons and holes. Isomorphic incorporation of transition metals into MCM-41 can produce photocatalysts that are even active under visible-light irradiation [17]. For example, MCM-41 containing Ti and other transition

* Corresponding author. Tel.: +86 22 27892340; fax: +86 22 27892340.
*E-mail address:* jj_zou@tju.edu.cn (J.-J. Zou).

0926-3373/$ – see front matter © 2010 Elsevier B.V. All rights reserved.
doi:10.1016/j.apcatb.2010.01.024

metal ions showed high activity for photocatalytic oxidation of organics and water splitting [18–20]. Titania loaded Cr–MCM-41 exhibited reasonable activity for photocatalytic organic elimination under visible light [21–25]. Our previous work already indicated that incorporating titanium into MCM-41 framework could produce highly active photocatalysts for NBD isomerization [16]. One can expect that introducing second transition metal ion into Ti–MCM-41 may generate more active photocatalyst. In this work, we incorporated transition metal ions (V, Fe and Cr) into Ti–MCM-41 and applied them in the photoisomerization of NBD.

## 2. Experimental

### 2.1. Photocatalysts synthesis

The photocatalysts were synthesized via a direct hydrothermal method, using cetyltrimethyl ammonium bromide (CTAB) as the structure director, and tetrathyorthosilicate (TEOS), tetrabutyl titanate (TBOT), vanadium sulfate ($VOSO_4$), chromium nitrate ($Cr(NO_3)_2$) and iron sulfate ($FeSO_4$) as the Si, Ti, V, Cr and Fe sources, respectively.

For M–Ti–MCM-41($x$) synthesis, the starting materials have a molar composition of CTAB:TEOS:TBOT:NaOH:M = 1:7.5$x$/(1.03 + $x$):0.225$x$/(1.03 + $x$):7.5/(1.03 + $x$):1.8, where $x$ is the Si/M atomic ratio. The initial Si/Ti ratio was 33 for all samples. Typically, V–Ti–MCM-41(75) was synthesized as follows: at 50 °C, 1.82 g CTAB was dissolved in a solution containing 50 mL deionized water and 0.42 g NaOH, and then 8.21 mL TEOS was added dropwise and stirred for 1 h. In the mixture 0.375 mL TBOT and 1 mL $VOSO_4$ solution (0.5 M) were sequentially added. The pH value was adjusted to 10.5–11.0 using NaOH solution (3 M) followed by stirring for 1 h. Then the resulting gel was transferred into a 90 mL Teflon-lined autoclave and heated at 100 °C for 72 h. The obtained powders were filtered, washed with deionized water, dried at 100 °C overnight and calcined in air at 500 °C for 5 h. For comparison, pure siliceous MCM-41 and Ti–MCM-41 were also synthesized using the same procedure.

### 2.2. Characterization

The bulk compositions of prepared materials were determined by energy-dispersive X-ray attached on a XL 30ESEM scanning microscope. Their crystal structures were assessed using a Rigaku D/max 2500 v/pc powder X-ray diffractometer equipped with a Cu Kα radiation source. The pore structures were evaluated through $N_2$ adsorption–desorption at −196 °C on a Micrometritics ASAP2010 system. The surface area and pore distribution were calculated using the BET and BJH methods, respectively. The morphologies of photocatalysts were observed using a Philips Tecnai G2 F20 electron microscope. The local structures of metal ions were evaluated using UV–vis diffusing reflecting spectra recorded in a Jasco UV-3600 spectrometer. XPS measurements were conducted using a Perkin-Elmer PHI1600-ECSA spectrometer to confirm the chemical state of metals. The binding energies were referenced to the C1s peak (284.6 eV) of surface adventitious carbon. IR spectra were also recorded on a Nicolet 560 FTIR spectrometer to get more structural information.

### 2.3. Photocatalytic reaction

The photocatalytic activities were evaluated in a closed cylindrical quartz vessel (550 mL) with inner irradiation. A 400 W high pressure mercury lamp (Tianjinruisente UV Company, China) was positioned inside the vessel and cooled by circulating water jacket. The maximum irradiation in the UV region was at 365 nm with intensity of 18 mW/cm$^2$. To conduct the reaction, a mixture containing 5 mL NBD, 500 mL p-xylene and 0.1 g photocatalysts was suspended in the vessel under magnetic stirring. A sample was withdrawn at regular intervals and analyzed using a HP 4890 gas chromatography equipped with a BP-1 capillary column (25 m × 0.33 mm × 0.05 μm) and a FID detector. The oxidation of NBD could not be completely excluded, but the possibility should be very small because there was no fresh oxygen supplied. In addition, the sample was analyzed using GC–MS (Agilent 6890N) with a HP-5 capillary column (30 m × 0.5 mm × 0.25 μm), and no oxidized intermediates were detected.

## 3. Results and discussion

### 3.1. Structural characteristics

EDX data shows that the bulk Si/Ti ratios in M–Ti–MCM-41 are in a narrow range of 55–70, agreement with the ratio of 66 in Ti–MCM-41. So the Ti content can be regarded as constant for all samples. As shown in Table 1, the bulk Si/Cr ratio is lower while the Si/Fe is higher than the initial values, but the discrepancy is in normal range. However, the V content in the prepared samples is significantly low, probably due to the slow hydrolysis rate of vanadium ions. XPS data shown in the parentheses reflect that the surface metal is less than the bulk composition. Similar tendency is

**Table 1**
Textural properties of M–Ti–MCM-41.

| Sample | $d_{100}$ (nm) | $a_0$ (nm) | $S_{BET}$ (m$^2$ g$^{-1}$) | Pore volume (cm$^3$ g$^{-1}$) | Pore size (nm) | Wall thickness (nm)[a] | Si/M ratio[b] |
|---|---|---|---|---|---|---|---|
| MCM-41 | 3.647 | 4.211 | 1176 | 0.78 | 2.60 | 1.61 | |
| Ti–MCM-41 | 3.709 | 4.283 | 1048 | 0.81 | 2.76 | 1.52 | |
| V–Ti–MCM-41(150) | 3.771 | 4.354 | 1005 | 0.81 | 2.79 | 1.56 | 298 |
| V–Ti–MCM-41(100) | 3.806 | 4.395 | 1020 | 0.83 | 2.81 | 1.58 | 196 |
| V–Ti–MCM-41(75) | 3.741 | 4.320 | 983 | 0.86 | 2.84 | 1.48 | 162 |
| V–Ti–MCM-41(33) | 3.906 | 4.510 | 932 | 0.88 | 2.96 | 1.55 | 87(102) |
| V–Ti–MCM-41(10) | 4.012 | 4.633 | 684 | 0.72 | 3.23 | 1.40 | 32(58) |
| Fe–Ti–MCM-41(150) | 3.873 | 4.472 | 1001 | 0.81 | 2.81 | 1.66 | 210 |
| Fe–Ti–MCM-41(100) | 3.978 | 4.493 | 982 | 0.82 | 2.88 | 1.61 | 106 |
| Fe–Ti–MCM-41(75) | 3.741 | 4.320 | 931 | 0.86 | 2.95 | 1.37 | 94 |
| Fe–Ti–MCM-41(33) | 3.977 | 4.592 | 858 | 0.83 | 3.02 | 1.57 | 48(93) |
| Fe–Ti–MCM-41(10) | 4.163 | 4.807 | 756 | 0.82 | 3.49 | 1.32 | 18(51) |
| Cr–Ti–MCM-41(150) | 3.870 | 4.469 | 952 | 0.80 | 2.83 | 1.63 | 131 |
| Cr–Ti–MCM-41(100) | 3.872 | 4.471 | 912 | 0.78 | 2.89 | 1.58 | 71 |
| Cr–Ti–MCM-41(75) | 3.711 | 4.285 | 874 | 0.76 | 2.98 | 1.30 | 66 |
| Cr–Ti–MCM-41(33) | 3.871 | 4.470 | 644 | 0.66 | 3.30 | 1.19 | 25(50) |
| Cr–Ti–MCM-41(10) | 3.977 | 4.592 | 419 | 0.62 | 4.81 | - | 10(33) |

[a] Wall thickness = unit cell size ($a_0$) − pore size.
[b] Values in the parentheses are detected by XPS.

also observed for Ti content. One can conclude that both the Ti and M ions are distributed in the inner layer of prepared materials, not enriched or aggregated on the surface.

Fig. 1 shows the XRD patterns of synthesized materials. MCM-41 has a strong peak at $2\theta = 2$–$3^\circ$ and two weak peaks at 4–5° corresponding to the (1 0 0), (1 1 0), and (2 0 0) reflexes of ordered hexagonal mesoporous structure, respectively. Ti–MCM-41 has very similar patterns, indicating that incorporating Ti into Si–O framework does not influence the ordered structure, agreed with previous result [16]. The peaks are also observed in the patterns of V- and Fe-incorporated samples, suggesting that the ordered structure is sustained after introduction of metal ions.

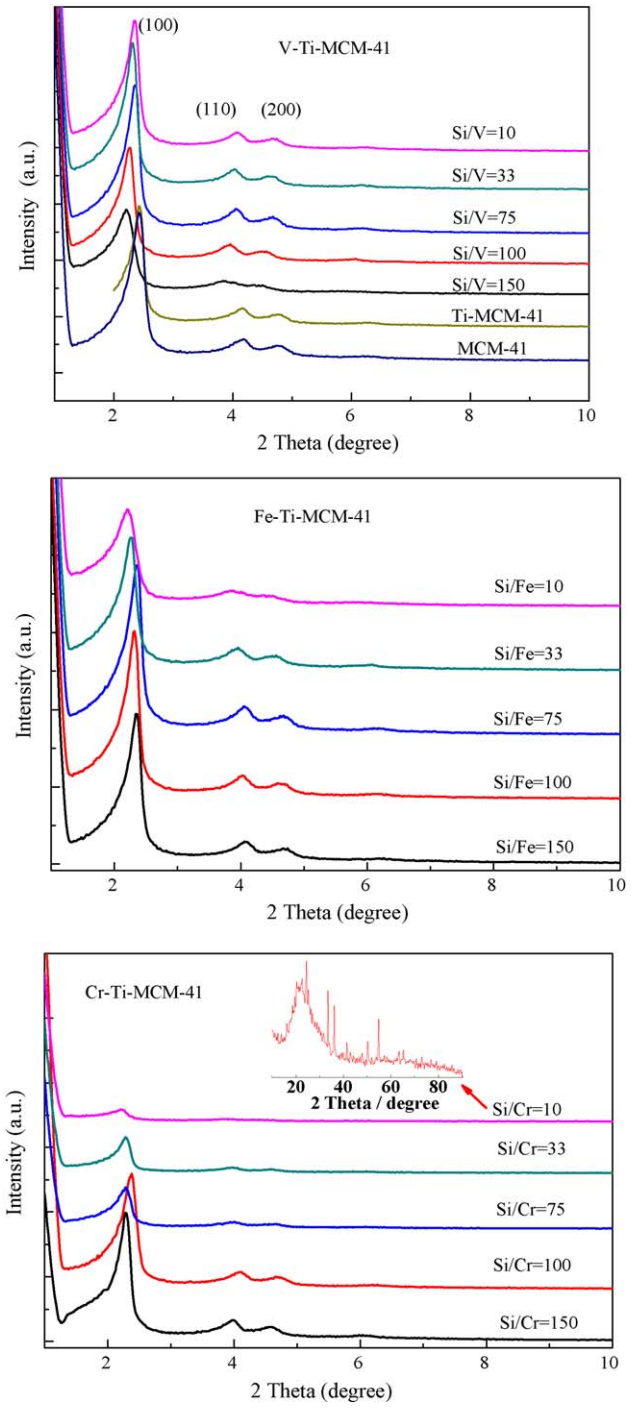


**Fig. 1.** Low-angle XRD patterns of M–Ti–MCM-41 (the inserted is the patterns of Cr–Ti–MCM-41(10) in $2\theta$ range of 5–90°).

However, they are weakened with the increase of metal content, which hints the presence of transition metal ions hinders the structure-directing action of template [21]. There are no any peaks assigned to metal oxides in the high-angle region (figure not shown), thus the metal ions are either atomically dispersed in the framework of MCM-41 or attained an amorphous form outside the framework. It is noted that the diffraction peaks shift towards low angle after introduction of V and Fe ions. As shown in Table 1, the $d_{100}$ spacing and cell size $\alpha_0$ are enlarged, which is attributed to the isomorphic substitution of framework Si atoms by metal ions. The parameters continuously increase with the metal content because more Si ions are substituted. It can be seen that most of the V and Fe ions are dispersed in the Si–O framework.

Introducing Cr ions significantly destroys the crystallinity of parent materials (see Fig. 1). When the Si/Cr ratio decreases to 10, the (1 0 0) reflex becomes extremely weak, and the (1 1 0) and (2 0 0) reflexes are no longer observable. Since the radius of Cr ion is the largest among the three metals studied, one may expect that incorporating Cr into Si–O framework will change the crystal structure more evidently. However, the shift of peaks and increase in cell parameters of Cr–Ti–MCM-41 are not as evident as those of V– and Fe–Ti–MCM-41. The reason is that the large ion radius hinder Cr ions get into the Si–O framework. So the amount of Cr ions incorporated in Si–O framework is very limited, and many of them are in the form of extraframework species. With very high Cr content, bulk metal oxides will present in the materials. As evidence, a peak at $2\theta = 22.5^\circ$ assigned to $Cr_2O_3$ particles is observed for Cr–Ti–MCM-41(10) [20,26]. These species exist between the interfaces of silica agglomerates and retard the crystal growth, thus the prepared materials show very weak diffractive patterns.

$N_2$ adsorption–desorption characterizations give type-IV isotherm (figure not shown) which is the characteristic of mesoporous materials. The adsorption at low pressures ($P/P_0 < 0.25$) is accounted for monolayer–multilayer adsorption of $N_2$ on the walls of mesopores. At relative pressure ($P/P_0$) between 0.25 and 0.45, a sharp inflection due to capillary condensation within mesopores appears. The sharpness in this step indicates a uniform pore size [27]. The inflection becomes less sharp and moves to higher pressure with increasing metal content, meaning the ordered mesoporous structure is destroyed and the pore size grows. Table 1 demonstrates the surface area decreases with the increase of metal content, whereas the pore volume and pore size increase. This result hints the collapse of pores and formation of distortions in the wall. The thickness of pore walls generally decreases compared with the parent materials, supporting that incorporating metal ions restrain the crystal integrity of MCM-41. Especially, Cr–Ti–MCM-41(10) has the smallest surface area and the largest pore size. Moreover, its wall thickness is negative because the pore size is even large than the unit cell. In this case, the material exists in amorphous rather than ordered structure.

Fig. 2 shows the high-resolution TEM images of some materials. When small amount of metal ions (Si/M ratio > 75) is introduced, the ordered structure is slightly disturbed. With the increase of metal content, some uniform pores collapse, confirming that incorporating metal ions interrupts the Si–O framework and weakens its integrity. Generally, V-incorporation just lowers the crystallinity slightly because the actual V content is very low and the ion radius is relatively small. On the contrary, Cr-incorporation dramatically destroys the ordered structure. When the Si/M ratio decreases to 10, the regular arrays are no longer observable. Specifically, Cr–Ti–MCM-41(10) is composed of some crystallites. These observations are in good agreement with the XRD and $N_2$ adsorption–desorption results.

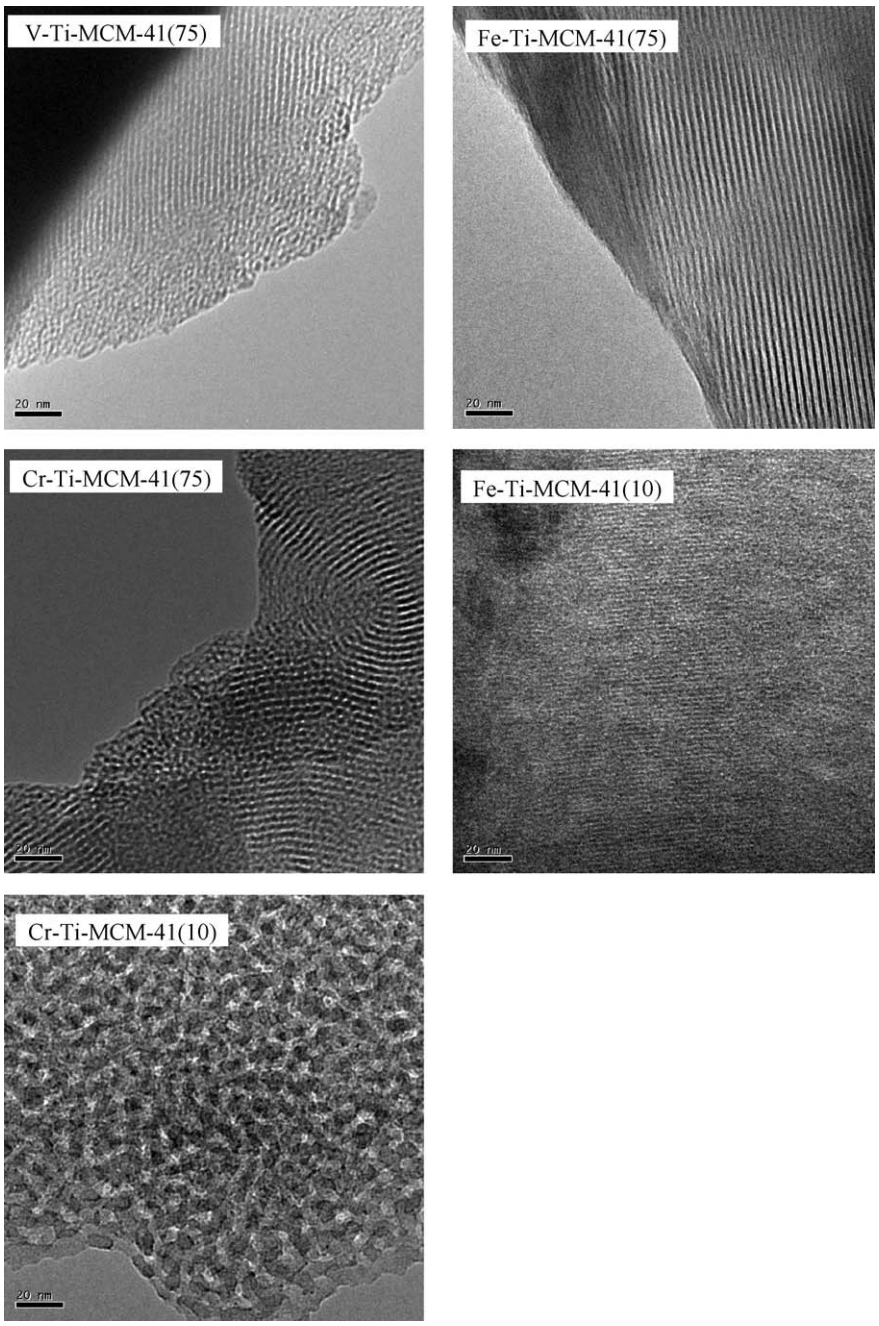


**Fig. 2.** TEM images of M–Ti–MCM-41.

### 3.2. Spectroscopic characteristics

Fig. 3 shows the UV–vis spectra of prepared samples. Ti–MCM-41 shows a broad absorption between 210 and 340 nm. The strongest absorption centered around 210–215 nm can be ascribed to the charge transfer from the lattice oxygen ($O^{2-}$) to Ti species in tetrahedral coordination. And the shoulder peak at 250–340 nm is assigned to Ti species in higher coordination environments [24,28]. V–Ti–MCM-41(150) shows very similar spectrum, without any absorption in the >330 nm region. It has been reported that the band around 258 is associated to $V^{5+}$ species in 4-fold coordination state [23,29]. One can conclude that V ions are highly dispersed in MCM-41 framework at atomic level with tetrahedral coordination. For V–Ti–MCM-41(100), an additional absorption around 370 nm assigned to $V^{5+}$ ions in 6-fold coordination appears. When more V ions are introduced, the prepared materials show absorption in the >400 nm region, indicating the formation of some species in higher coordination or even polymerized environments [19,29]. Fe–Ti–MCM-41 with Si/Fe ratio below 75 shows absorption below 400 nm, which is the evidence of $Fe^{3+}$ ions in 4- and 8-fold coordination [30,31]. So the Fe ions are also isomorphously incorporated into the Si–O framework. Fe–Ti–MCM-41(10) has a strong absorption between 400 and 600 nm which is the characteristic of $Fe_2O_3$ species [30].

Cr–Ti–MCM-41(150) shows two bands at 275 and 350 nm representing the $O^{2-} \rightarrow Cr^{6+}$ charge transfer of tetrahedrally coordinated Cr-oxide moieties [22,32]. A weak shoulder around 430 nm assigned to $Cr^{6+}$ polychromate also presents in the spectrum [27,29]. With the increase of Cr content, two bands at 470 and 610 nm that are the characteristics of poly- and bulk $Cr_2O_3$ become intensive. It is clear that the order of dispersion extent for the three metal ions is V > Fe > Cr.

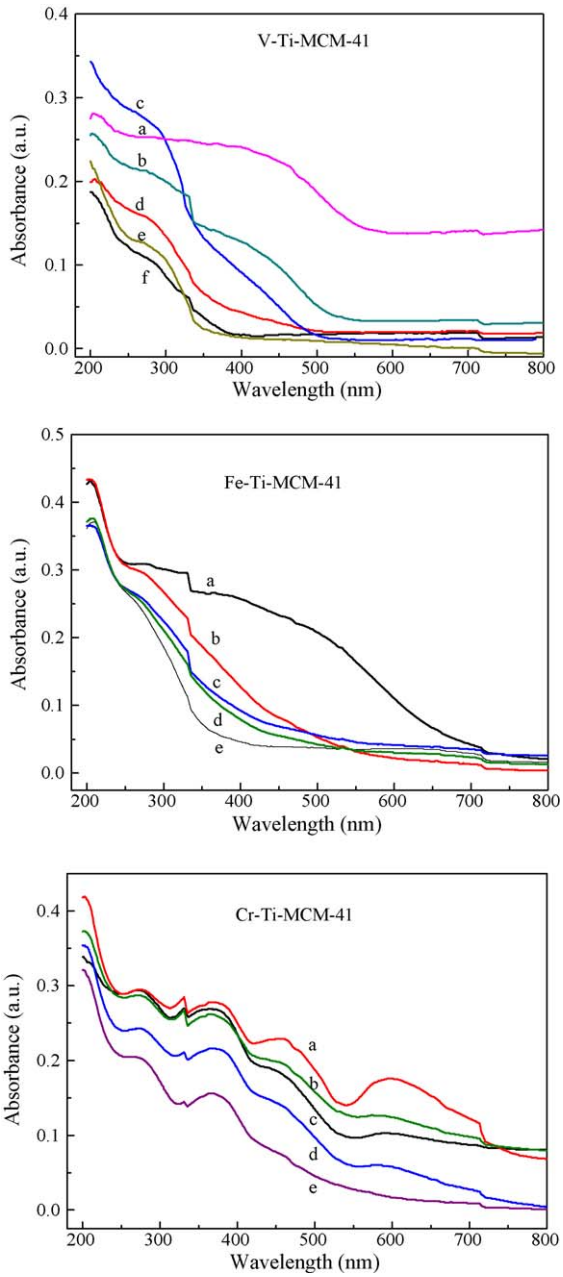


**Fig. 3.** UV–vis diffuse reflecting spectra of M–Ti–MCM-41 (a, b, c, d and e represents sample with Si/M ratio of 10, 33, 75, 100 and 150, respectively. f represents Ti–MCM-41).

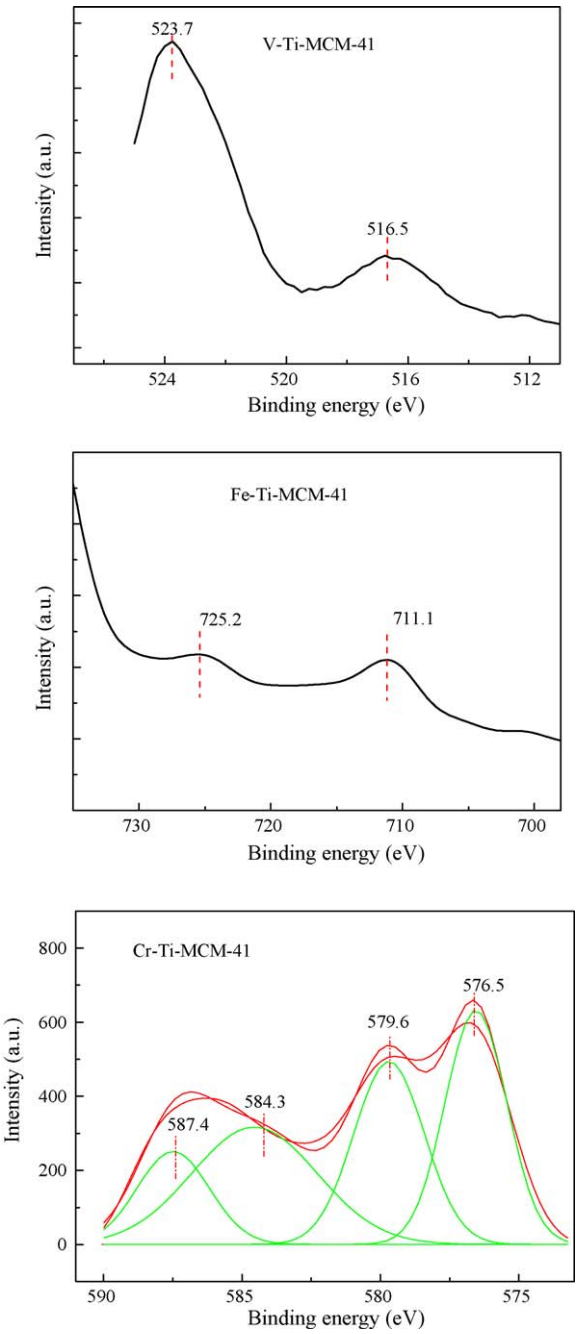


**Fig. 4.** Metal XPS spectra of M–Ti–MCM-41(10).

XPS characterizations in Fig. 4 further confirm the chemical state of metal ions. When the Si/M ratio is higher than 33, there is no metal detectable because of its low concentration. The binding energies of V are 523.7 and 516.5 eV for $2p_{1/2}$ and $2p_{3/2}$ splits, respectively, and the difference is about 7.2 eV, in agreement with the reported values of $V^{5+}$ ions [29]. For Fe-incorporated materials, the binding energies of 725.2 and 711.1 eV are assigned to $2p_{1/2}$ and $2p_{3/2}$ splits of $Fe^{3+}$ ions [30]. These peaks are broad compared with the narrow lines of bulk oxides, which is taken as the evidence of highly dispersed metal ions in silica framework [29]. The Cr peak is significantly broad and asymmetrical, indicative of multiple chemical states. Fitting the curve gives two Cr species or chemical states. The peaks at 576.5 and 584.3 eV are assigned to $2p_{3/2}$ and $2p_{1/2}$ of $Cr^{3+}$ species, whereas those at higher binding energy of 579.6 and 587.4 eV are referred to $Cr^{5+}$ ions [21,22].

IR spectra in Fig. 5 also give some information on the structure of prepared samples. MCM-41 exhibits a band around 970 $cm^{-1}$ been interpreted in terms of Si–OH groups. Ti- and metal-incorporated samples also show this band. However, a careful check on them shows that it is shifted to 960 $cm^{-1}$. Moreover, this band becomes more intensive with increasing metal content when taken the symmetric vibration of Si–O–Si bond at ~800 $cm^{-1}$ as reference. One may also notice the Si–O–Si band at 1090 $cm^{-1}$ shifts to 1083–1086 $cm^{-1}$ after the introduction of meal ions, which is more obvious with increasing metal content. These observations can be used as the indicator of Ti and M ions incorporated in Si–O framework [19,20,26,27,33]. There are no signals of V or Fe ions due to the high dispersion extent. However, Cr–Ti–MCM-41 shows a shoulder band at 880–900 $cm^{-1}$ assigned to $Cr^{6+}$ species [26,27]. For Cr–Ti–MCM-41(10), two new bands at

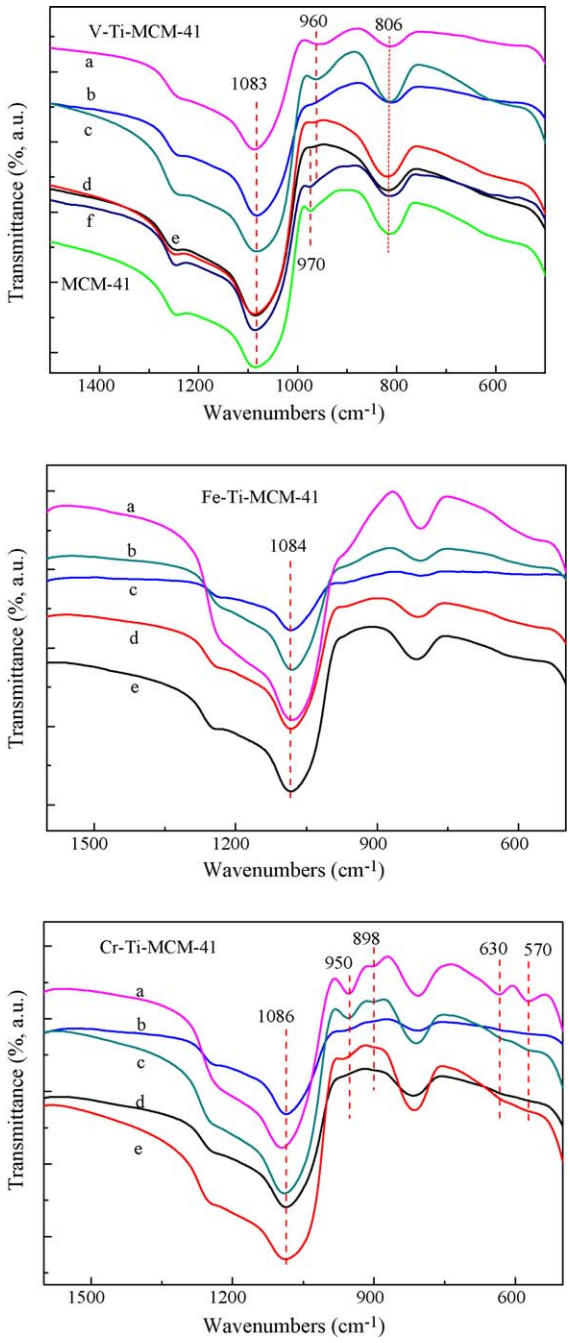


**Fig. 5.** IR spectra of M–Ti–MCM-41 (a, b, c, d and e represents sample with Si/M ratio of 10, 33, 75, 100 and 150, respectively. f represents Ti–MCM-41).

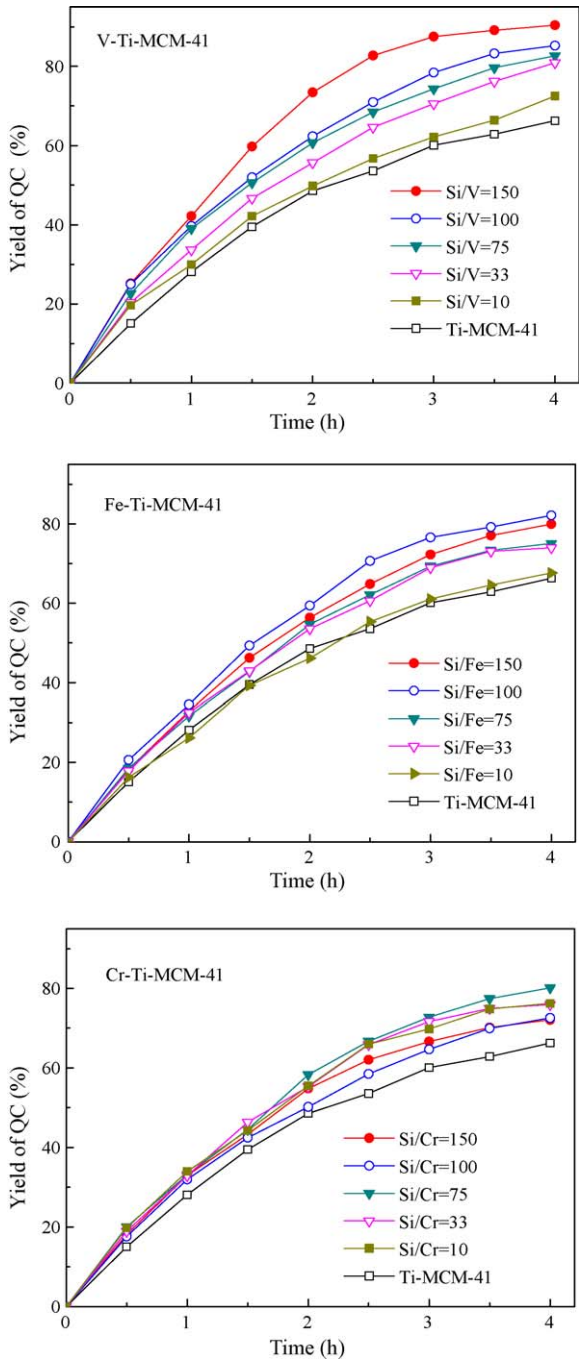


**Fig. 6.** Photocatalytic performances of M–Ti–MCM-41 under UV irradiation.

630 and 570 $cm^{-1}$ belonging to extraframework $Cr_2O_3$ oxides are also observed [26,34], confirming the formation of $Cr_2O_3$ species.

### 3.3. Photocatalytic activity

The yield of QC is used to evaluate the photoisomerization activity of prepared materials under UV irradiation (see Fig. 6). All the materials exhibit higher activity when compared with Ti–MCM-41, indicating that introducing second metal is beneficial to the photoisomerization. For V-incorporated samples, the activity rises up with the increase of Si/V ratio, and V–Ti–MCM-41(150) shows a specifically high activity. The activity of Fe–Ti–MCM-41 also increases along with the Si/Fe ratio, but the discrepancy is not as evident as the V-incorporated counterparts. Cr–Ti–MCM-41 has irregular performance in a narrow range, with the order of Si/Cr(75) > Si/Cr(33) ≈ Si/Cr(10) > Si/Cr(150) ≈ Si/Cr(100). On the whole, V-incorporation is most effective for the photoisomerization, Fe-incorporation follows, and Cr-incorporation is the least.

Photocatalyst characterizations have shown that the primary Ti ions are homogeneously dispersed in Si–O framework as isolated species, and the dispersion state is not influenced by the introduction of second metal. The amount of transition metals ions is less than that of Ti ions in the prepared materials in most case. Specifically, the highly active V–Ti–MCM-41 possesses only trace amount of V ions. With this consideration, it is believed that Ti–O species are the active sites for the photoisomerization, and the second transition metal ions serves as additive to improve the activity.

Data in Fig. 6 suggests that the photocatalytic activity have nothing to do with the concentration of second transition metal ions. The improvement in the activity should be related to their extent of dispersion and local structure. Tetrahedrally coordinated M-oxide moieties like V, Cr and Fe dispersed in mesoporous materials can be easily excited under UV and/or visible-light irradiation to form corresponding charge-transfer excited states [17,18,25,32]:

$$[M^{n+} - O^{2-}] \xrightarrow{h\nu} [M^{(n-1)+} - O^{-}]^{*} \quad (M = V, Cr, Fe)$$

Davydov et al. reported that, the $Cr^{5+}$ species of $[Cr^{5+} - O^{-}]^{*}$ can donate an electron into the surrounding Ti–O moieties and $O^{-}$ can scavenge an electron from the surrounding Ti–O moieties [21]. In this case, the charge separation will occur with a hole and an electron in Ti–O species. If this process happens at or near the photocatalyst surface, the charges can induce photoisomerization. Considering Cr, V and Fe ions have the same electronic structure, one can expect the same charge transition happen on $[V^{4+} - O^{-}]^{*}$ and $[Fe^{2+} - O^{-}]^{*}$ excited states. Therefore, two different excitation mechanisms exist in M–Ti–MCM-41. One is the direct excitation of Ti–O moieties by UV irradiation, and the other is the indirect excitation via charge transition from $[M^{(n-1)+} - O^{-}]^{*}$ states. The indirect excitation caused by the presence of second transition metal ions should be responsible for the high photocatalytic activity because of its high efficiency in charge formation and separation.

The different activities of photocatalysts can be explained by the local structure of metal ions and textural characteristics of particles. For V–Ti–MCM-41(150), the majority of $V^{5+}$ ions are highly dispersed in 4-fold coordination, which brings up highly efficient excitation of Ti–O species. Its well retained ordered structure and high surface area can enhance the adsorption of NBD molecules and provide more active sites. Therefore this photocatalyst possess very high activity. With the increase of V content, some 4-fold ions are transformed into undesirable species in higher coordination and even polymerized environments. On the contrary, the damaged structure and small surface area may suppress the concentration and adsorption of reactants. As a result, the activity is decreased with the increase of metal content. The tendency of Fe-incorporated samples is also attributed to these reasons. As to Cr–Ti–MCM-41, the chromium ions are badly dispersed in various forms, and the weight of framework $Cr^{6+}$ is very low. Moreover, the ordered structure is seriously destroyed. Thereby its activity is relatively low.

Since some photocatalysts show absorption in visible-light region, one may wonder whether they exhibit activity under visible-light irradiation. So the photocatalytic reaction was conducted under visible irradiation (>420 nm). Unfortunately, there is no observable conversion. This is different from the case of $H_2$ generation and organic elimination, where Cr–Ti–MCM-41 is reported to exhibit visible-light activity [18,20,21]. We have suggested that the photoisomerization of NBD may occur through the exciplex (charge-transfer) intermediate formed between excited Ti–O and NBD species [15,16], which is different from the well-studied photocatalytic oxidation and reduction. The absence of visible activity is probably due to the different reaction mechanism between the photoisomerization and other photocatalytic reactions.

## 4. Conclusions

V, Fe and Cr incorporated Ti–MCM-41 materials have been prepared via hydrothermal method and used as photocatalysts for the photoisomerization of norbornadiene. At low metal content, $V^{5+}$ and $Fe^{3+}$ ions are well dispersed in the Si–O framework with tetrahedral coordination. Some species in higher coordination or even polymerized environments present with increasing metal content, and the ordered structure is slightly damaged. Cr ions are difficult to be incorporated into the framework, with various species like extraframework $Cr^{6+}$ and bulk oxides formed, which dramatically destroys the ordered structure. The metal-incorporated materials show improved photocatalytic activity under UV irradiation, with the role order of V- > Fe- > Cr-incorporation. Tetrahedrally coordinated metal ions dispersed in Si–O framework may play an important role in the excitation of Ti–O species. V–Ti–MCM-41(150) is most active, attributed to high dispersion of 4-fold coordinated $V^{5+}$ ions and well retained ordered mesoporous structure.

## Acknowledgments

The authors greatly appreciate the supports from the National Natural Science Foundation of China (20906069), the Foundation for the Author of National Excellent Doctoral Dissertation of China (200955), and the Research Fund for the Doctoral Program of Higher Education of China (200800561011).

## References

[1] A.D. Dubonosov, V.A. Bren, V.A. Chernoivanov, Russ. Chem. Rev. 71 (2002) 917–927.
[2] D.P. Schwendiman, C. Kutal, Inorg. Chem. 16 (1977) 719–721.
[3] R.D. Bach, I.L. Schilke, H.B. Schlegel, J. Org. Chem. 61 (1996) 4845–4847.
[4] M. Rosi, A. Sgamellotti, Inorg. Chem. 38 (1999) 1520–1522.
[5] M.Z. Kassaee, E. Vessally, S. Arshadi, J. Mol. Struct.: THEOCHEM 763 (2006) 13–19.
[6] J. Chen, L. Zhang, Y.-Y. Li, J. Chen, G. Yang, Y. Li, J. Photochem. Photobiol. A 185 (2007) 67–75.
[7] P.A. Cahill, R.N. Steppel, US Patent 20040031675 (2004).
[8] H.-F. Fan, T.-L. Chin, K.-C. Lin, J. Phys. Chem. B 108 (2004) 9364–9370.
[9] C. Qin, Z. Zhao, S.R. Davis, J. Mol. Struct.: THEOCHEM 728 (2005) 65–70.
[10] S.J. Schneider, AIAA-98-3670 (1998).
[11] S.D. Bai, P. Dumbacher, J.W. Cole, NASA/TP-2002-211729 (2002).
[12] S.J. Schneider, US Patent 6311477 (2001).
[13] R.C. Striebich, J. Lawrence, J. Anal. Appl. Pyrolysis 70 (2003) 339–352.
[14] T.S. Kokan, J.R. Olds, J.M. Seitzman, P.J. Ludovice, Acta Astronautic 65 (2009) 967–986.
[15] J.-J. Zou, B. Zhu, W. Li, X. Zhang, Z. Mi, J. Mol. Catal. A 286 (2008) 63–69.
[16] J.-J. Zou, M.-Y. Zhang, B. Zhu, W. Li, X. Zhang, Z. Mi, Catal. Lett. 124 (2008) 139–145.
[17] M. Matsuoka, M. Anpo, J. Photochem. Photobiol. C 3 (2003) 225–252.
[18] H. Yamashita, K. Yoshizawa, M. Ariyuki, S. Higashimoto, M. Che, M. Anpo, Chem. Commun. (2001) 435–436.
[19] Y. Hu, N. Wada, K. Tsujimaru, M. Anpo, Catal. Today 120 (2007) 139–144.
[20] S. Shen, L. Guo, Catal. Today 129 (2007) 414–420.
[21] L. Davydov, E.P. Reddy, P. France, P.G. Smirniotis, J. Catal. 203 (2001) 157–167.
[22] B. Sun, E.P. Reddy, P.G. Smirniotis, Appl. Catal. B 57 (2005) 139–149.
[23] E.P. Reddy, L. Davydov, P.G. Smirniotis, J. Phys. Chem. B 106 (2002) 3394–3401.
[24] Y.-J. Do, J.-H. Kin, J.-H. Park, S.-S. Park, S.-S. Hong, C.-S. Suh, G.-D. Lee, Catal. Today 101 (2005) 299–305.
[25] F.C. Marques, M.C. Canela, A.M. Stumbo, Catal. Today 133–135 (2008) 594–599.
[26] S.V. Awate, N.E. Jacob, S.S. Deshpande, T.R. Gaydhankar, A.A. Belhekar, J. Mol. Catal. A 226 (2005) 149–154.
[27] Z. Zhu, Z. Chang, L. Kevan, J. Phys. Chem. B 103 (1999) 2680–2688.
[28] X. Wang, W. Lian, X. Fu, J.-M. Basset, F. Lefebure, J. Catal. 238 (2006) 13–20.
[29] R.K. Jha, S. Shylesh, S.S. Bhoware, A.P. Singh, Micropor. Mesopor. Mater. 95 (2006) 154–163.
[30] A. De Stefanis, S. Kaciulis, L. Pandolfi, Micropor. Mesopor. Mater. 99 (2007) 140–148.
[31] Q. Zhang, Q. Guo, X. Wang, T. Shishido, Y. Wang, J. Catal. 239 (2006) 105–116.
[32] S. Rodrigues, K.T. Ranjit, S. Uma, I.N. Martyanov, K.J. Klabunde, J. Catal. 230 (2005) 158–165.
[33] O.A. Anunziata, A.R. Beltramone, J. Cussa, Catal. Today 133–135 (2008) 891–896.
[34] I.P. Saraswat, A.C. Vajpei, J. Mater. Sci. Lett. 3 (1984) 515–517.